Macromolecules

ARTICLE

pubs.acs.org/Macromolecules

Precise Analyses of Short-Time Relaxation at Asymmetric Polystyrene Interface in Terms of Molecular Weight by Time-Resolved Neutron Reflectivity Measurements

Daisuke Kawaguchi,[†] Andrew Nelson,[‡] Yuichi Masubuchi,[§] Jaroslaw P. Majewski,[⊥] Naoya Torikai,[∥] Norifumi L. Yamada,[#] A. R. Siti Sarah,[†] Atsushi Takano,[†] and Yushu Matsushita[*,†]

[†]Department of Applied Chemistry, Nagoya University, Furo-cho, Chikusa-ku, Nagoya 464-8603, Japan

[‡]Australian Nuclear Science and Technology Organisation, Locked Bag 2001, Kirrawee DC, NSW, 2232 Australia

[§]Institute for Chemical Research, Kyoto University, Gokasho, Uji 611-0011, Japan

[⊥]Los Alamos Neutron Science Center, Los Alamos National Laboratory, Los Alamos, New Mexico 87545, United States

[∥]Department of Chemistry for Materials, Mie University, 1577 Kurimamachiya-cho, Tsu, 514-8507, Japan

[#]Neutron Science Division, Institute for Materials Structure Science, High Energy Acceleration Research Organization, 203-1 Shirakata, Tokai, Naka 319-1106, Japan

Supporting Information

ABSTRACT: The short-time mutual diffusion at an interface of linear polystyrene/linear deuterated polystyrene with different molecular weights was examined by time-resolved neutron reflectivity (TR-NR) measurements. The model scattering length density (b/V) profiles obtained by solving a partial differential equation for the diffusion process, using the segmental diffusion coefficients as the only fitting parameter were used to analyze the TR-NR data. In short-time diffusion, the asymmetric (b/V) profiles derived from a segmental relaxation model were able to model the data much better than those obtained by center-of-mass diffusion based on reptation model and by a simple error function. These analyses clearly indicate that even if the molecular weights of both components are larger than the critical molecular weight for entanglement, the initial interfacial broadening of bilayer films with different molecular weight proceeds with asymmetric mobility being proportional to N^{-1}. Time dependence of the interfacial positions, $u(t)$, was extracted from the (b/V) profiles. The exponent of α in $u(t) \sim t^{\alpha}$ reflects the asymmetric mobility of the components. This analysis also gave the time dependence of mutual diffusion coefficients, D. The D value gradually decreases with increasing time and reaches a constant value.

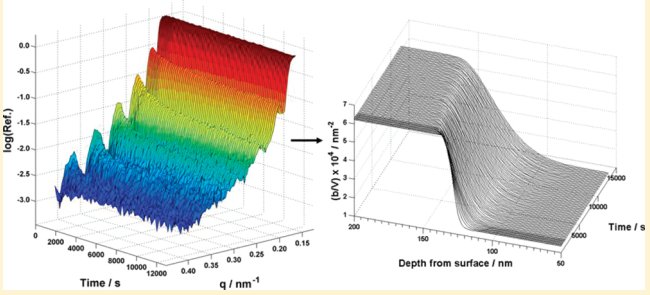

INTRODUCTION

Understanding the mobility of polymers at interfaces is crucial to the optimization of adhesion, welding, crack healing, *etc*. Since diffusion behavior at interfaces directly reflects the molecular motion of polymers, it has been studied from the viewpoint of polymer dynamics as well as engineering for many years. The simplest diffusion couple is composed of polymer and its deuterated counterpart with same molecular weight. Studies of these symmetric interdiffusion systems have revealed that dynamics of linear polymers can be described using reptation theory.[1−3] However, molecular-scale mutual diffusion when there is asymmetry of molecular weight, component and topology *etc* is still an open question.

The mutual diffusion of polymers has been investigated by a variety of methods and can be summarized in terms of depth resolution, probe particles/radiations and contrast to distinguish each of the components.[4] Depending on the depth resolution, nuclear reaction analysis,[5−7] dynamic secondary ion mass spectroscopy,[8−17] and neutron reflectivity, NR,[18−30] are classified as techniques for measuring concentration profiles on the order of molecular size. In comparison with these methods, infrared spectroscopy,[31,32] Rutherford backscattering[33,34] and forward recoil spectroscopy,[35,36] are done as techniques for measuring diffusion distances at length scales much greater than molecular size. Among these techniques, NR is one of the most powerful tools to investigate polymer interdiffusion because of their superior depth resolution (less than 1 nm). In the past the majority of NR measurements on bilayer samples has been conducted in a static fashion by annealing and quenching for a certain length of time as the speed of measurement has been relatively slow. However, static measurements are not appropriate for the detection of small changes in concentration profiles as differences in the initial

Received: July 25, 2011
Revised: October 13, 2011
Published: November 04, 2011

states of the interfaces leads to unacceptable experimental uncertainty. Thus, it is desirable that time evolution of concentration profiles of individual sample is measured by time-resolved neutron reflectivity (TR-NR) measurements.

TR-NR measurements of interdiffusion were first used for examination of symmetric polystyrene/deuterated polystyrene, and asymmetric oligo-styrene/polystyrene bilayer systems by Bucknall et al.[27] In the symmetric bilayer film, NR data can be analyzed with a simple Fickian model in which a constant diffusion coefficient is independent of matrix concentration and the concentration profile is described by a symmetric error function. On the other hand, the NR profiles for the asymmetric bilayer film were analyzed with an asymmetric model scattering length density (b/V) profile in which two error functions were convoluted, as a symmetric error function was unsuccessful. In this case, diffusion coefficients could not be extracted directly from the concentration profiles at each time because the concentration profile was not calculated based on a physical model.

Karim et al. investigated the short-time interdiffusion of bilayers composed of hydrogenous and deuterated polystyrenes with nearly same degree of polymerizations using NR.[18,20] Since the NR analyses based on (b/V) profiles with a simple error function cannot reproduce experimental NR profiles even in the nearly symmetric case, two error functions were convolved in the model (b/V) profiles. Furthermore, they deduced the diffusion coefficients of PS from time evolution of interfacial thickness squared. However, these analyses can be only conducted under the assumption that the diffusion coefficient is constant through a certain time range. If the NR profiles are analyzed with physically accurate models (b/V), more universal analyses can be conducted.

The objective of this study is to elucidate the interdiffusion behavior of polystyrene bilayer films with different molecular weights by TR-NR measurements. We demonstrate the utility of the combination of TR-NR measurements and analyzing the data using concentration profiles obtained by the solution of the diffusion equation.

EXPERIMENTAL SECTION

Samples. Linear deuterated polystyrene (l-dPS) was prepared by a living anionic polymerization under vacuum. Four linear normal polystyrenes (l-hPS) were purchased from Tosoh Corp. Weight-average molecular weight, M_w, of l-dPS was obtained by multiangle laser light scattering (MALLS) measurement using DAWN EOS from Wyatt Technology Inc. Molecular weight distribution, M_w/M_n, of l-dPS was evaluated by gel permeation chromatography (GPC) on Tosoh HLC-8020 system equipped with DP-8020 pump, refractive index detector (RI-8020) and three TSK gel columns ($G4000H_{HR} \times 3$). The columns were calibrated with polystyrene standards. Glass transition temperatures, T_g, were determined by differential scanning (DSC) calorimetric measurements on EXSTAR 6100 from SII Nanotechnology Inc., calibrated with Indium and water standards. The heating rate is 10 K min^{-1} and the second scan was used. The molecular characteristics of polymers used in this study are listed in Table 1 where N is degree of polymerization.

l-hPS/l-dPS bilayer films were prepared by a floating method described as follows.[12,13] l-dPS films were prepared by spin-coating onto 3 in.-diameter and 3 mm-thick silicon wafers with native oxide layer from toluene solutions. The l-dPS films were annealed at 150 °C for at least 48 h under vacuum. Second, l-hPS films were prepared onto silicon wafers by spin-coating method from toluene solutions and subsequently floated off onto water surface. The l-hPS films were picked up onto the l-dPS films from the air-side. The l-hPS/l-dPS bilayer films were dried at room temperature under vacuum for 48 h.

Table 1. Characteristics of Polystyrenes Used in This Study

sample code	M_w	N	M_w/M_n	T_g/K
l-dPS-127k	127K	1.13×10^3	1.04	378.9
l-hPS-1090k	1090K	1.05×10^4	1.08	381.1
l-hPS-427k	427K	4.11×10^3	1.02	380.3
l-hPS-190k	190K	1.83×10^3	1.04	379.7
l-hPS-96.4k	96.4K	9.27×10^2	1.01	378.0

The film thicknesses of the bottom l-dPS layers and the bilayers were evaluated by X-ray reflectivity (XR) measurements using an ATX-G thin-film diffractometer operating with Cu Kα radiation (λ =0.154 nm). The thicknesses of the bottom l-dPS layers were measured before preparing the bilayer, with the thicknesses of top l-hPS layers being obtained by subtracting the bottom layer thicknesses from the total bilayer film thickness (XR cannot differentiate between d/h PS as they both have the same electron density). The XR data were analyzed using Motofit.[37] Table 2 shows the l-hPS/l-dPS bilayer films and their initial thicknesses where d_t and d_b are thicknesses of top and bottom layers, respectively.

Time-resolved specular neutron reflectivity (TR-NR) measurements were performed on two different reflectometers: (a) SPEAR[38] (Los Alamos Neutron Science Center, Los Alamos National Laboratory, U.S.), with polychromatic wavelengths, λ, ranging from 0.15 to 1.6 nm, a sample−detector distance $D_{s\text{-}d}$ = 3670 mm; (b) ARISA-II[39] (BL-16, Materials and Life Science Facility, Japan Proton Accelerator Research Complex, Tokai, Japan), with polychromatic wavelengths ranging from 0.20 to 0.88 nm, $D_{s\text{-}d}$ = 1777 mm. The modulus of the neutron momentum transfer vector in NR is

$$q_z = \frac{4\pi}{\lambda} \sin\theta \quad (1)$$

where θ is the angle of specular reflection. θ values were set to ca. 1.2° and 0.55° to obtain the q ranges $0.16 < q < 1.7$ nm^{-1} and $0.15 < q < 0.7$ nm^{-1} for SPEAR and ARISA-II, respectively.

For TR-NR experiments, the cell was maintained at a set temperature ranging from 389 to 408 K and the incident angle was fixed before putting a sample. After checking the temperature of the cell, a bilayer sample was put into the cell. It was confirmed that the temperature at the top surface of a bilayer film reached an equilibrium temperature within a few minutes. After that, the cell was evacuated using a diaphragm pump (oil free) to prevent oxidation of the sample. NR profiles were then collected by every 3 min.

RESULTS AND DISCUSSION

Analyses of NR Profiles. Figure 1 shows typical TR-NR profiles of l-hPS-427k/l-dPS-127k bilayer films (annealed at 405 K) as a function of time (An animated plot is given in Supporting Information. The changes in shape of fringes were more clearly observed.). In this bilayer sample, the fringe spacing is predominantly determined by the thickness of the l-dPS-127k layer since the contrast of (b/V difference) between air and l-hPS-427k is smaller than that between l-hPS-427k and l-dPS-127k. The top l-hPS-427k layer is only visible through the distortions of the interference fringes. At the initial stage of interdiffusion, the fringes are well-defined in the q range 0.15−0.4 nm^{-1}. As annealing process proceeds, the fringes at higher q become increasingly damped. This clearly indicates that the diffusion occurs at the l-hPS-427k/l-dPS-127k interface. In general, since the information on interfaces appears in high q region, NR

Table 2. Thicknesses of Bilayer Samples at Room Temperature Used in This Study

sample code	Bilayer (top/bottom)	top layer thickness, d_t/nm	bottom layer thickness, d_b/nm
bilayer 1	l-hPS-427k/l-dPS-127k	124.6 ± 0.9	104.8 ± 0.5
bilayer 2	l-hPS-427k/l-dPS-127k	124.3 ± 0.8	103.7 ± 0.7
bilayer 3	l-hPS-427k/l-dPS-127k	121.8 ± 1.5	114.7 ± 0.5
bilayer 4	l-hPS-190k/l-dPS-127k	134.9 ± 0.2	92.6 ± 0.2
bilayer 5	l-hPS-190k/l-dPS-127k	115.4 ± 0.4	97.4 ± 0.2
bilayer 6	l-hPS-96.4k/l-dPS-127k	122.1 ± 0.4	102.2 ± 0.3
bilayer 7	l-hPS-1090k/l-dPS-127k	153.9 ± 0.5	96.6 ± 0.4

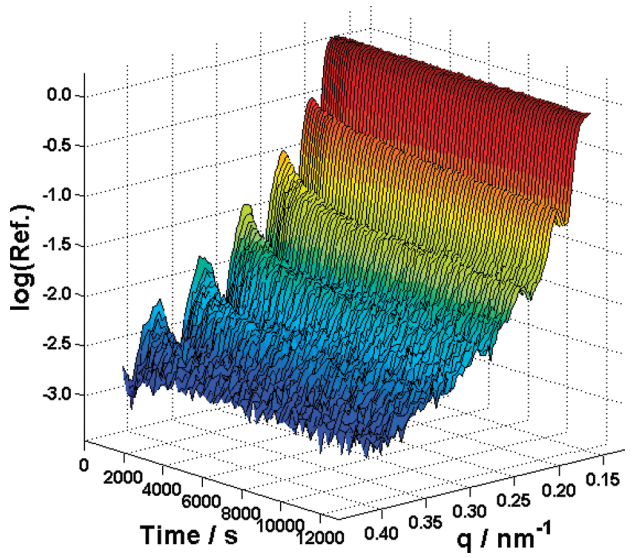

Figure 1. Time-resolved neutron reflectivity profiles for l-hPS-427k/l-dPS-127k bilayer film (bilayer 1) annealed at 405 K.

profiles in high q should be analyzed to evaluate the early stage of interdiffusion. However, we noticed that the changes in the shape of fringes were observed even in the low q range. This is because the position of the interface shifts with increasing time. Furthermore, this phenomenon becomes remarkable when the asymmetry of the mobility increases. Therefore, we claim that asymmetric interdiffusion can be analyzed by TR-NR profiles even in the limited q range.

Neutron reflectivity profiles were analyzed using on an interdiffusion model proposed by Jabbari and Peppas.[40] We refer the reader to their paper for greater detail although we describe it briefly here. The model is based on irreversible thermodynamics and accounts for the composition dependence of tracer diffusion coefficients, assuming the monomeric friction coefficients of the two polymers are identical. One phase consists of the polymer with low mobility (designated by s for "slow") with vacancies randomly distributed in the lattice. The other phase consists of the polymer with high mobility (designated by f for "fast"). It is assumed that the concentration of vacancies is a small fraction of total concentration and does not contribute to the free energy of mixing. Since the polymers on each side of the interface have different molecular weights and chemical structures (even with the isotopic counterparts), there is a chemical potential gradient across the interface. The system is modeled by using this chemical potential gradient as the driving force for the interdiffusion. Various physical models can be applied for the NR analysis by using the corresponding Onsager coefficients. Here, we compare the reptation model that they used, a segmental motion model modified by us and the conventional symmetric error function.

(i). Symmetric Error Function (Method i). Here the asymmetric mobility is ignored. Interdiffusion at an asymmetric interface shows not only the change in NR profiles in high q range but also in the shape of the fringes in low q range. This method is used for showing how differs the experimental and calculated NR profiles if asymmetric mobility ignores. In the simplest analysis the diffusion coefficient, D, is treated as constant independent of matrix concentration. The solution to Fick's second law with constant D results in a symmetric error function. The concentration profile with respect to the z-axis is given by:

$$\phi = \frac{1}{2}\mathrm{erfc}\left(\frac{z}{\sqrt{2Dt}}\right) \tag{2}$$

(ii). Reptation Model (Method ii)[40,45]. On the basis of reptation theory, the partial differential equation describing the diffusion process at the interface between two compatible polymers can be expressed in the following form after differentiation with respect to the z axis (see Appendix in the Supporting Information):

$$\frac{\partial \phi_s}{\partial t} = D\frac{\partial^2 \phi_s}{\partial z^2} + \frac{\partial D}{\partial \phi_s}\left(\frac{\partial \phi_s}{\partial z}\right)^2 \tag{3}$$

$$D = D_0\left(\frac{1-\phi_s}{N_s} + \frac{\phi_s}{N_f}\right)\left(\frac{1-\phi_s}{N_s} + \frac{\phi_s}{N_f} + 2\chi_{sf}\phi_s(1-\phi_s)\right) \tag{4}$$

where φ_s, N_s, N_f, and χ_{sf} are the volume fraction of slower component, the degree of polymerization of slower and faster components and the Flory−Huggins interaction parameter between slower component and faster one, respectively. In this system, the χ_{sf} value is negligibly small. D_0 is the diffusion coefficient for the entanglement segment and can be described as

$$D_0 = \frac{RTN_e}{f_m} \tag{5}$$

where N_e, f_m, R and T are the degree of polymerization of entanglement segments, the friction coefficient of the monomeric unit, gas constant and temperature, respectively. The initial and boundary conditions for solving the above diffusion equations are:

$$t = 0\ \varphi_f = 0 \quad \text{for} \quad 0 \le z < d_s \tag{6}$$

$$t = 0\ \varphi_f = 1 \quad \text{for} \quad d_s \le z \le d_s + d_f \tag{7}$$

$$z = 0\ \partial\varphi_f/\partial z = 0 \quad \text{for} \quad t > 0 \tag{8}$$

$$z = d_s + d_f\ \partial\varphi_f/\partial z = 0 \quad \text{for} \quad t > 0 \tag{9}$$

where d_s and d_f are the film thicknesses of slower and faster components, respectively. It is important to recognize the importance of each term on the right-hand side of eq3. The first term represents interdiffusion at the interface between the two polymers while the second term represents the swelling of the slower-moving component by the faster-moving component.[40] Another feature is that the interface, defined as the depth at $\varphi_s = 0.5$, shifts toward the faster component side with time in model ii due to the asymmetric flux while the interface remains in the same position in model i.

(iii). Rouse Model (Method iii). A polymer chain in the Rouse model is represented as N beads connected by springs. Since this model can describe segmental motion, we tried NR fitting analysis using the Rouse model. The diffusion equation in this model can be expressed as (see the Appendix in the Supporting Information):

$$\frac{\partial\phi_s}{\partial t} = D\frac{\partial^2\phi_s}{\partial z^2} + \frac{\partial D}{\partial\phi_s}\left(\frac{\partial\phi_s}{\partial z}\right)^2 \tag{10}$$

$$D = D_0'\left(\frac{1-\phi_s}{N_s} + \frac{\phi_s}{N_f} + 2\chi_{sf}\phi_s(1-\phi_s)\right) \tag{11}$$

$$D_0' = \frac{6RT}{f_m} \tag{12}$$

Again, this partial differential equation can be solved using the initial and boundary conditions of eq6−9. By comparing eq4 and eq11, D is proportional to N^{-2} in the reptation model while D is proportional to N^{-1} in the Rouse model. Hence, the asymmetry of mobility at the interface is reduced in the model iii. The interface in the model iii also moves toward the faster component side.

Calculation of Model (b/V) Profiles. Concentration profiles were obtained by eq2 and by solving the above differential equations numerically. In the numerical calculation, the segment size a and the segmental diffusion time $t_0 = a^2/D_0$ are chosen as unit of length and time, respectively. The segment size a has been determined as 0.67 nm[41] while the segmental diffusion coefficient D_0 remains as a fitting parameter. A concentration profile was converted into a scattering length density, (b/V), profile using (b/V) values of l-hPS and l-dPS at an annealing temperature. The (b/V) values of l-hPS and l-dPS were calculated by the following equation

$$\left(\frac{b}{V}\right) = \frac{\rho N_A \sum_i b_i}{M} \tag{13}$$

where ρ, b_i, N_A, and M are mass density, a coherent scattering length of component i, the Avogadro's number and molecular weight of monomeric unit, respectively. To take mass density at an annealing temperature into consideration, the temperature dependence of ρ (in g cm^{-3}) for l-hPS was estimated by the reported equation as follows.[42]

$$\rho = 1.0865 - 6.19\times10^{-4}\times(T-273) + 0.136\times10^{-6}\times(T-273)^2 \tag{14}$$

Table 3. Fixed Parameters for NR Analyses

sample	temp/K	d_t/nm	d_b/nm	χ_{sf}
bilayer 1	405	127.3	107.1	2.04×10^{-4}
bilayer 2	395	126.4	105.5	2.16×10^{-4}
bilayer 3	389	123.4	116.3	2.24×10^{-4}
bilayer 4	398	137.4	94.3	2.13×10^{-4}
bilayer 5	390	117.0	98.8	2.22×10^{-4}
bilayer 6	398	124.4	104.1	2.13×10^{-4}
bilayer 7	408	157.4	98.9	2.00×10^{-4}

For l-dPS, ρ value was simply multiplied by 1.08 (= 112/104, weight ratio of monomeric unit of styrene-d_8/styrene-h_8). A film thickness of each layer at a temperature is estimated by the following equation[43] and the value is fixed through the NR analysis

$$\left(\frac{d_T}{d_0}\right) - 1 = (T_g - T_0)\times1.1\times10^{-4} + (T - T_g)\times5.1\times10^{-4} \tag{15}$$

where d_T and d_0 are film thicknesses at T and T_0 (=room temperature), respectively. The temperature dependence of χ_{sf} for l-hPS/l-dPS pair is given by the following relation:[44]

$$\chi_{sf} = -(2.9\pm0.4)\times10^{-4} + (0.20\pm0.01)T^{-1} \tag{16}$$

In our analysis, a χ_{sf} value is obtained by eq 16 and treated as a fixed parameter. Although the χ_{sf} value was used in the analysis, the value is negligibly small for this system. The theoretical reflectivity of a model (b/V) profile is then calculated and compared to the data. D in method i, D_0 in method ii, and D_0' in method iii are the only fitting parameters in each analysis. Fitting to the data used a least-squares fitting metric in Motofit.[37] The fixed parameters of each bilayer film used in this study are listed in Table 3.

Model Comparison. Figures 2(a)∼(c) show selected NR profiles of l-hPS-427k/l-dPS-127k bilayer film annealed at 405 K (bilayer 1) for 4.8×10^2 s, 1.4×10^3 s, 2.4×10^3 s, 6.1×10^3 s, and 1.2×10^4 s. The (b/V) profiles shown in Figure 2, parts d−f, are calculated using models i−iii, respectively. When the flux of l-hPS-427k is equal to that of l-dPS-127k at $\varphi_s = 0.5$ (model i), the fringes of the calculated reflectivity profiles simply dampen as with increasing time, but the position of the fringe top is maintained (Figure 2a). In this case, the agreement between the experimental and the calculated reflectivities becomes increasingly worse with time. This means that NR has high sensitivity to detect a slight change in the interfacial position. On the other hand, when the flux is asymmetric at $\varphi_s = 0.5$ (models ii and iii), the position of the fringe top shifts with increasing time as shown in Figure 2, parts b and c. The experimental reflectivities are in good agreement with the calculated ones in cases ii and iii, indicating that the model (b/V) profiles are physically realistic. The initial interface is located at 127.3 nm from the surface drawn by the solid line. The (b/V) profiles gradually broaden with increasing time. The shapes of the (b/V) profiles in Figure 2, parts e and f, are asymmetric; the (b/V) profiles on the l-hPS side (left-hand side) are broader than those in the l-dPS side (right-hand side). Furthermore, the interfacial position defined at $\varphi_s = 0.5$ shifted toward l-dPS side with time in models ii and iii. These results clearly indicate that the flux of low molecular weight

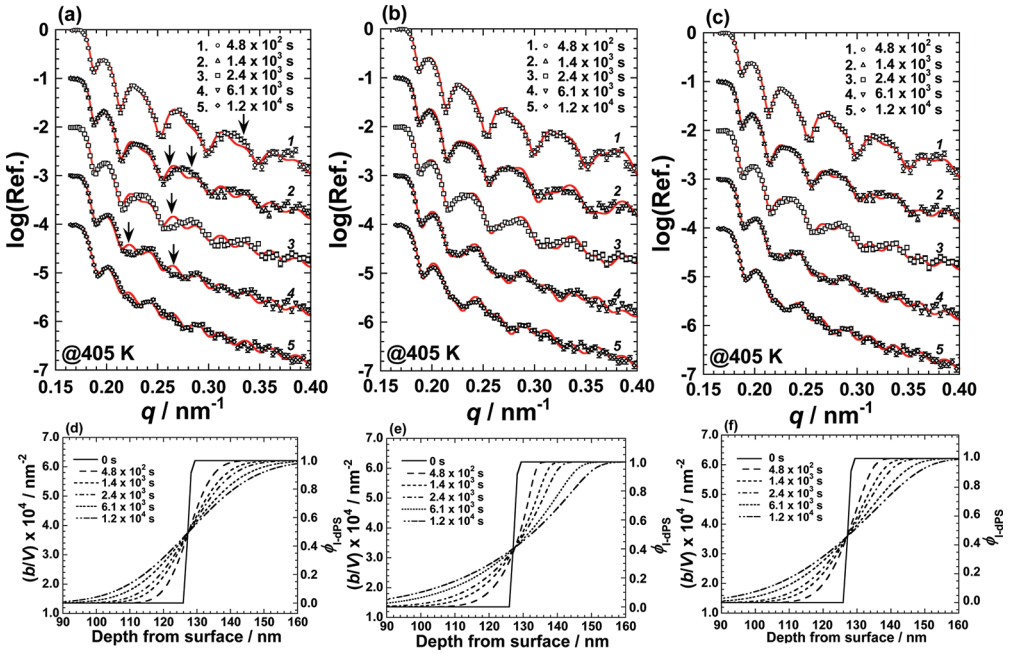

Figure 2. Selected NR profiles (a−c) (vertically offset for clarity) and model (b/V) profiles (d)∼(f) for l-hPS-427k/l-dPS-127k bilayer film annealed at 405 K(bilayer 1). Symbols in NR profiles are experimental reflectivities and solid lines are the calculated ones. Parts a−c are the calculated reflectivities obtained by the model (b/V) profiles shown in (d) (method i), (e) (method ii), and (f) (method iii), respectively.

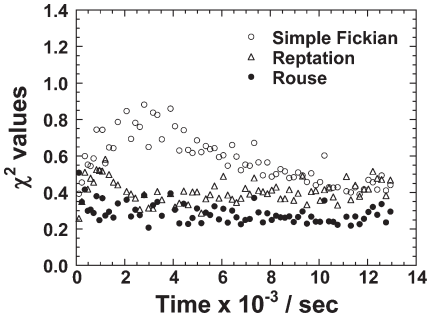

Figure 3. Time dependence of χ^2 values for NR profile analyses using methods i−iii.

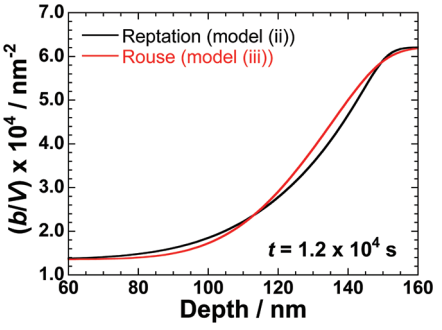

Figure 4. Comparison of the model (b/V) profiles calculated using models ii and iii. These (b/V) profiles give best-fit NR curves at $t = 1.2 \times 10^4$ s.

component (l-dPS) is larger than the high molecular weight one (l-hPS) at the interface and they are qualitatively consistent with the fast-mode theory.[46]

To judge which model is the most proper, χ^2 values which correspond to the sum of the squared differences between the experimental and calculated reflectivities are evaluated. Figure 3 shows the χ^2 values of NR analyses using methods i−iii as a function of time. The χ^2 values for method iii are the smallest among the three analysis methods. Hence, this comparison shows that the (b/V) profile obtained by solving the diffusion equation of the Rouse model reproduces the measured data most closely.

Theoretically, the reptation model ought to fit the data rather than Rouse model when the time is sufficiently longer than the reptation time of the slower component. Here, the reptation times for the faster and slower components for bilayer 1 are 1.0×10^2 and 4.8×10^3 s, respectively (The calculation of the reptation time is explained in the latter section.). However, it should be noted that the (b/V) profile obtained using model (ii) is calculated starting from an ideal flat interface as an initial condition. This (b/V) profile is different from the calculated one assuming that the transition from Rouse to reptation models occurs at a certain time.

Figure 3 indicates that although the χ^2 value of model ii is approaching to that of model iii after the reptation time of the slower component, the χ^2 value of model iii is still smaller than that of model ii. This means that the actual (b/V) profile is closer to that calculated using model iii than model ii. Comparing the (b/V) profiles calculated using models ii and iii at $t = 1.2 \times 10^4$ s shown in Figure 4, the depth at which the (b/V) value starts to decrease is almost the same, but the shape of the (b/V) profile in model iii is more gradual than that one in model ii. This means that the actual (b/V) profile after the reptation time of the slower component is still strongly affected by an early stage of interdiffusion obeying Rouse model. Therefore, it seems reasonable to hypothesize that the interfacial layer is formed by early stage of interdiffusion obeying Rouse model and the number density of

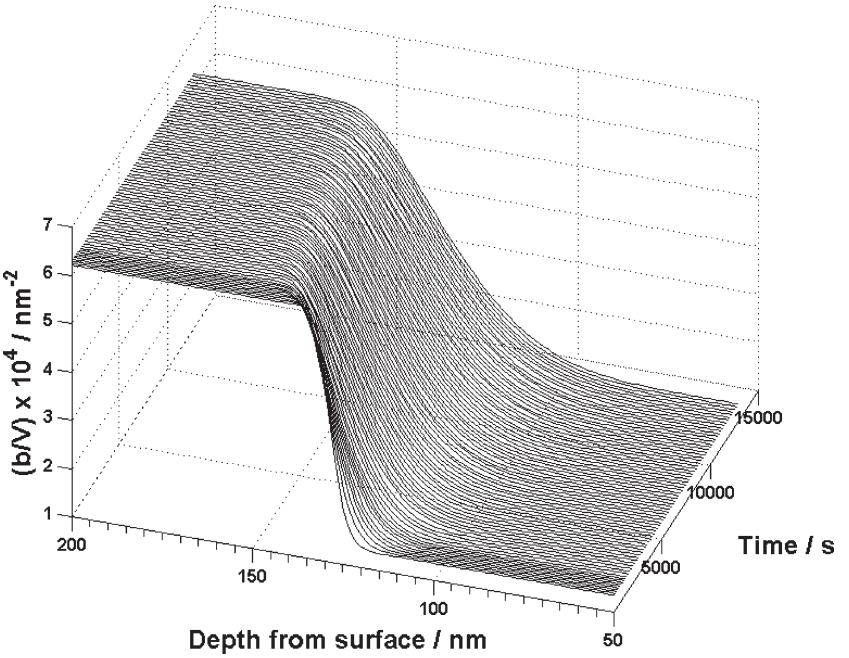

Figure 5. Time evolution of (b/V) profiles of l-hPS-427k/l-dPS-127k bilayer film annealed at 405 K.

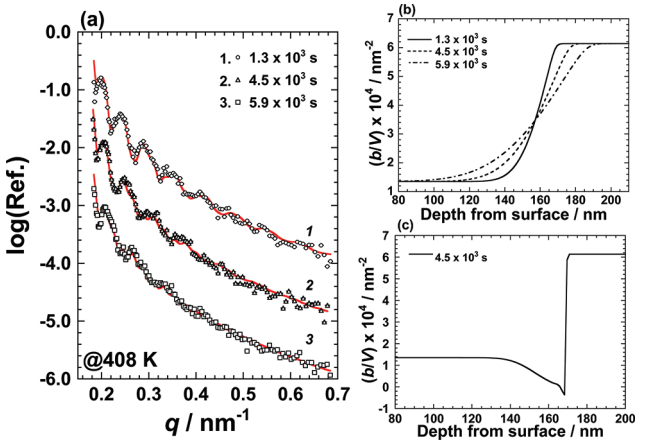

Figure 6. Selected NR profiles (a) and model (b/V) profiles (b) for bilayer 7. The model (b/V) profiles calculated based on method iii. (c) An example of unrealistic model (b/V) profiles calculated using model ii.

entanglement in the interfacial region reaches the bulk value and the transition from Rouse to reptation occurs. To confirm this hypothesis, we discuss interdiffusion of highly asymmetric bilayer film in the next section.

Figure 5 shows the time dependence of model (b/V) profiles for l-hPS-427k/l-dPS-127k bilayer films annealed at 405 K. These (b/V) profiles are obtained by solving diffusion equation of method (iii). On the basis of the Rouse model, the asymmetric depth profile is generated by the asymmetric mobility of two components being proportional to N^{-1} (the animation of time variation of the (b/V) profiles is shown in Supporting Information).

Highly Asymmetric Bilayer Film. To confirm the adaptability of this analysis, interdiffusion of bilayer films with higher asymmetry was examined. The N_s/N_f of the bilayer 7 is ca. 10 while this ratio of bilayer 1 is 4. Figure 6a shows the selected NR profiles for bilayer 7. The symbols represent experimental reflectivities and the solid lines are calculated ones obtained by using the Rouse model shown in Figure 6b. The method iii models the experimental reflectivities with good agreement. We tried to analyze NR profiles by using method ii, however, realistic concentration profiles could not be obtained. Figure 6c shows an example of a model (b/V) profile calculated using model ii. In the calculation, a large D_0 value is required to fit the NR data because D is proportional to N^{-2} in model ii. In this case, the mass flux of the faster component (l-dPS) is much greater than that of the slower component (l-hPS) so that the slower component is piled up near the interface and that the φ_s value near the interface exceeds the unity. This mutual diffusion phenomenon is physically impossible. Hence, it is confirmed by this analysis that, even if the molecular weights of components are asymmetric and the both are larger than the critical molecular weight for entanglement, the initial interfacial broadening of bilayer films with different molecular weight proceeds with asymmetric mobility being proportional to N^{-1}.

The Shift of the Interfacial Position. We now turn to the time dependence of interfacial positions. Before discussing this issue, the reptation time, τ_d, in bulk was estimated by the following equation:[2]

$$\tau_d = \frac{R^2}{3\pi^2 D} \tag{17}$$

Here R is the end-to-end distance of a polymer chain and is scaled as $(N)^{1/2}a$. a being the statistical segment length of PS and it is estimated to be 0.67 nm as mentioned before.[41] The empirical equation of the temperature and molecular weight dependence of diffusion coefficients of PS in bulk is expressed in the following two equations:[21,47]

$$\log\left(\frac{D}{T}\right) = A - \frac{B}{T - T_V} \tag{18}$$

$$A = -9.49 - 2\log\left(\frac{M}{255000}\right) \tag{19}$$

dx.doi.org/10.1021/ma201717e |Macromolecules 2011, 44, 9424–9433

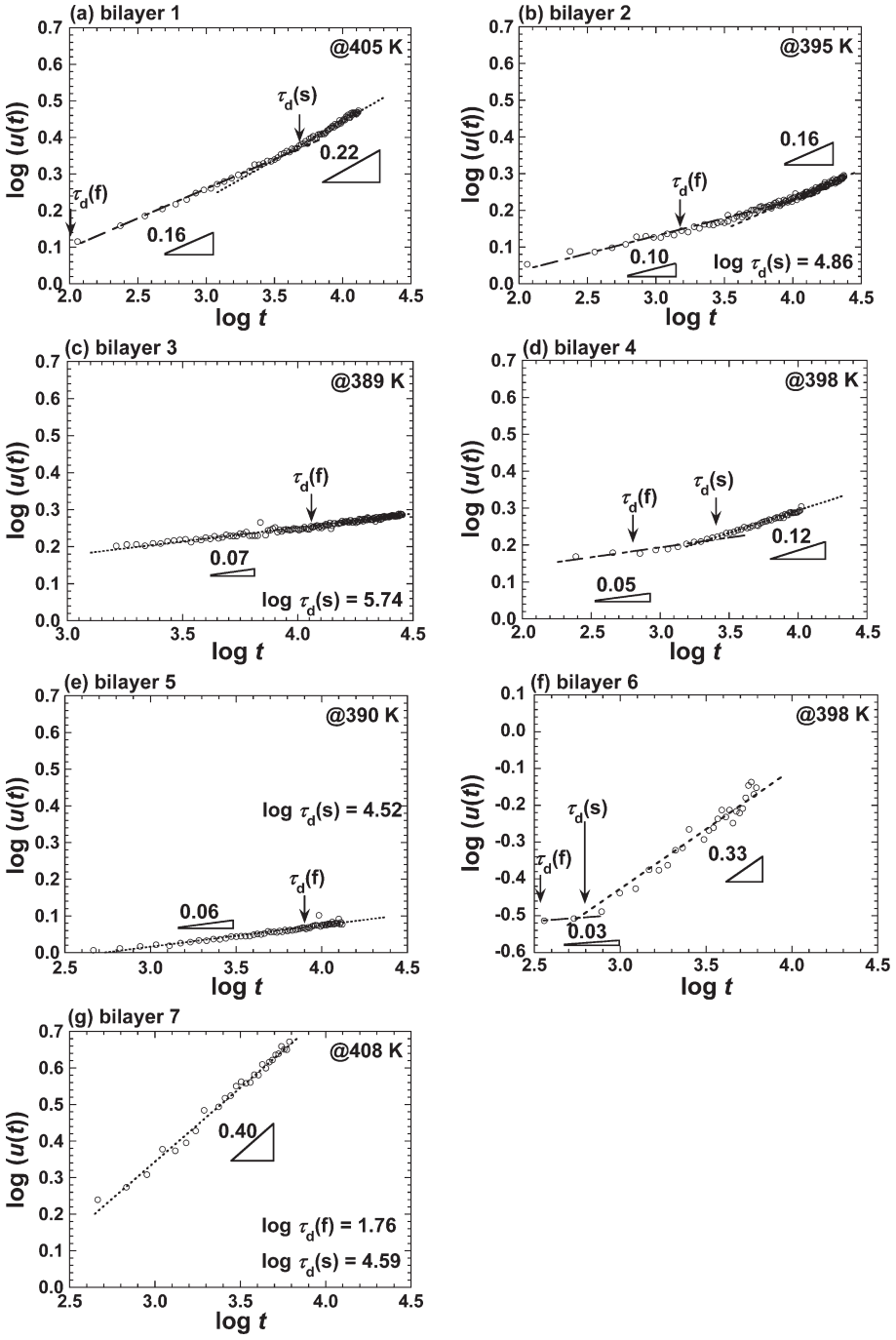

Figure 7. Double logarithmic plots of displacement of the interfacial position and time for various bilayers. The reptation times for the faster and slower components can be calculated from eqs 17−19.

B and T_v are the activation temperature and Vogel temperature, respectively. In bulk l-PS, the values of B and T_V are 710 and 322 K, respectively.[21,47]

The interfacial position of a l-hPS/l-dPS bilayer film is defined as the depth at $\varphi_s = 0.5$. An interfacial position moves with increasing time toward the faster component side when the flux at an interface is asymmetric. Displacement of an interfacial position, $u(t)$ (in nm), is defined as a difference between the interfaces at t and $t = 0$. Here, the positive value of $u(t)$ denotes that the interface moves the lower molecular weight component side (the faster component side). According to the reptation theory, the $u(t)$ is proportional to $t^{3/4}$ for $t < \tau_d$ and $t^{1/2}$ for $t > \tau_d$.[3] On the other hand, $u(t)$ is proportional to t^1 in case II diffusion, which is the most asymmetric interdiffusion.[48,49] In contrast, when an interdiffusion takes place at a perfectly symmetric interface, $u(t)$ is equal to 0. Hence, the exponent α in $u(t) \sim t^{\alpha}$ indicates the asymmetry of the mobility.

Figure 7 shows double logarithmic plots of $u(t)$ and t for various bilayer films. The reptation times for the faster and slower components (τ_d(f) and τ_d(s)) calculated from eqs 17∼19 are indicated by arrows in each graph. The more asymmetric the molecular weights are, the larger the absolute value of $u(t)$ is.

dx.doi.org/10.1021/ma201717e |*Macromolecules* 2011, 44, 9424–9433

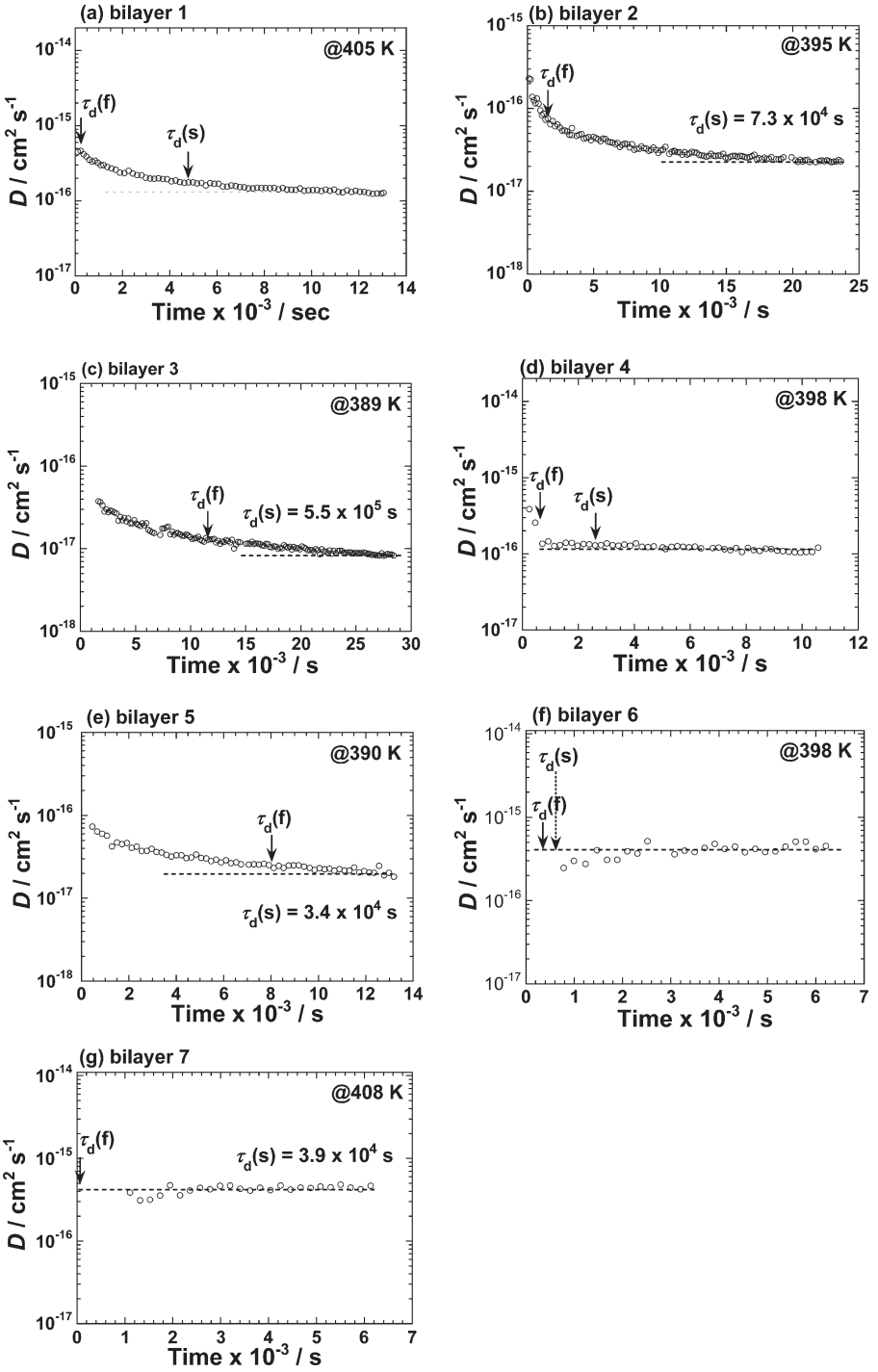

Figure 8. *D* vs time for various bilayer films.

In all cases, the $u(t)$ value increases with time, meaning that the interface moves toward the faster component side. Parts a−c of Figure 7 compare log $u(t)$ vs t for l-hPS-427k/l-dPS-127k bilayer films annealed at different temperatures. Bilayer 3 (Figure 7c) is the lowest annealing temperature and corresponds to the earliest stage of interdiffusion. This time region is around τ_d(f) and much shorter than τ_d(s). The α value is 0.07, indicating that the very early stage of interdiffusion is independent of asymmetry of molecular weight. The α value rises to 0.16 for $\tau_d(f) < t < \tau_d(s)$ and further increases to 0.22 for $t > \tau_d(s)$ as shown in Figure 7, parts a and b, meaning that the asymmetry of the mobility increases with increasing time and that a transition gradually occurs around τ_d(s). Comparing the α values of various bilayers for $\tau_d(f) < t < \tau_d(s)$, the α value increases with asymmetry of the molecular weights. On the basis of this analysis and the analyses of NR profiles in the previous section, it is likely that interdiffusion at asymmetric polymer interfaces proceeds by Rouse model at short time and gradually transitions to the reptation mode around τ_d(s). The α values for $\tau_d(f) < t < \tau_d(s)$ are less than 3/4 for all the bilayers and are not in agreement with the prediction

dx.doi.org/10.1021/ma201717e |*Macromolecules* 2011, 44, 9424–9433

Table 4. D, and D_0' Values at the Bilayer Interfaces

sample	temp/K	D/cm^2 s^{-1}	D_0'/cm^2 s^{-1}
bilayer 1	405	$(1.4 \pm 0.1) \times 10^{-16}$	$(2.1 \pm 0.1) \times 10^{-13}$
bilayer 2	395	$(2.5 \pm 0.1) \times 10^{-17}$	$(3.1 \pm 0.2) \times 10^{-14}$
bilayer 3	389	$(9.0 \pm 0.5) \times 10^{-18}$	$(1.3 \pm 0.7) \times 10^{-14}$
bilayer 4	398	$(1.2 \pm 0.1) \times 10^{-16}$	$(1.5 \pm 0.1) \times 10^{-13}$
bilayer 5	390	$(2.2 \pm 0.2) \times 10^{-17}$	$(2.7 \pm 0.2) \times 10^{-14}$
bilayer 6	398	$(4.0 \pm 0.7) \times 10^{-16}$	$(4.0 \pm 0.7) \times 10^{-13}$
bilayer 7	408	$(4.2 \pm 0.5) \times 10^{-16}$	$(7.2 \pm 0.8) \times 10^{-13}$

based on the reptation theory. This may be because the interdiffusion occurs by Rouse mode at short time and because the number density of entanglement near the interface increases with interdiffusion in reality while the number density is treated as a constant and same as that in the bulk in the theory.

Diffusion coefficients. Figure 8 compares time dependence of D values for various bilayer films. The D values are calculated by eq11 using $\varphi_s = 0.5$ and the D_0' values which give the best-fit NR profiles.

Let us consider bilayer 1 to start with. Figure 8(a) shows that the D value gradually decreases with increasing time and reaches a constant value of 1.4×10^{-16} cm^2 s^{-1} at long time limit. The reptation times of the faster and slower components, τ_d(f) and τ_d(s), for bilayer 1 are 1.0×10^2 and 4.8×10^3 s, respectively. The similar time dependence of D values was observed in Figure 8, parts b−e). On the other hand, the D values were constant through the time in Figure 6, parts f and g. Karim et al. reported that in nearly symmetric bilayer films, the D value decreases with time when t is shorter than τ_d and reaches a constant value at $t > \tau_d$.[18] This means that steady-state interdiffusion proceeds at $t > \tau_d$ while segmental relaxation is dominant at short-time region. We missed the transition—either because it happened too early in our experiments or because we did not wait long enough.

Table 4 lists the asymptotic D and D_0' values at long time limit when diffusion coefficients become constant. Unfortunately, it is not sufficient to discuss molecular weight dependence of D or D_0' values because the temperatures are different in each measurement. Since the temperatures are close to the T_g, small difference in the temperature can lead to the large difference in mutual diffusion coefficient.

Mutual diffusion was studied by other groups using rheological measurements on sandwich-like bilayer or coextruded multilayers.[50,51] Coextruded multilayers of a pair of high-density and linear low density polyethylenes are sheared by small amplitude oscillation between parallel plates.[51] The complex viscosity increased with time and the whole viscosity curve can be divided into three stages. At the beginning, the viscosity increases rapidly, then, the rate is gradually reduced in the second stage and transitions to the third stage, where the viscosity of both samples approaches a saturated value.[51] An increase in the viscosity at the second and third stages is in good agreement with the estimated one using partial differential equation based on reptation theory. However, the initial stage could not be measured because mutual diffusion can be naturally occurred during the coextrusion and the sample loading and melting in the rheometer. Their results cannot be compared with our results directly, however it is expected that the first stage of viscosity curve is closely related to the short-time diffusion presented in our study. Furthermore, time evolution of lap-shear strengths at bilayer interfaces was examined below the bulk T_g by Boiko and co-worker[52,53] and Akabori and co-workers,[54] separately. Both studies reveal that the activated segmental motion contributes to the increase in the lap-shear strength. However, the relationship between the formation of an entanglement and the mechanical response at the interface is still unclear and will lead to understanding the mechanism of adhesion.

CONCLUSIONS

We demonstrated time-resolved neutron reflectivity measurements of linear polystyrene/linear deuterated polystyrene bilayer films with different molecular weights. NR profiles were analyzed by solving the diffusion equation for the reptation and the segmental motion models using the mutual diffusion coefficient of segments, D_0 or D_0', as a fitting parameter, respectively. The time evolution of the scattering length density profiles near the interface can be obtained over a wide time scale. At short annealing time, D gradually decreases, before reaching an asymptotic value at longer times. Time dependence of the interfacial positions, $u(t)$, was extracted from the (b/V) profiles. The exponent of α in $u(t) \sim t^{\alpha}$ reflects the asymmetric mobility of the components. The combination of NR measurements and solution of the partial differential diffusion equation is a very good protocol to examine segmental relaxation and/or the interdiffusion.

ASSOCIATED CONTENT

Supporting Information. Animated plots of a TR-NR profile and a model (b/V) one and an appendix containing the calculations of diffusion equations. This material is available free of charge via the Internet at http://pubs.acs.org.

AUTHOR INFORMATION

Corresponding Author

*Telephone: +81-52-789-4604. Fax: +81-52-789-3210. E-mail: yushu@apchem.nagoya-u.ac.jp.

ACKNOWLEDGMENT

This research was in part supported by the grant-in-aids for young scientist (A)(No.22685013) and scientific research (A)(No.22245038), the Global COE program "Elucidation and Design of Materials Molecular Functions" from the Ministry of Education, Culture, Sports, Science and Technology (MEXT), Japan. This work benefited from the use of the SPEAR at the Lujan Neutron Scattering Center at Los Alamos Neutron Science Center funded by the DOE Office of Basic Energy Sciences and Los Alamos National Laboratory under DOE Contract DE-AC52-06NA25396. Neutron reflectivity measurements were also performed on BL-16 at the Materials and Life Science Facility, J-PARC, Japan, under the program number of 2009S08. D.K. thanks Mr. Hikage for assistant of X-ray reflectivity measurements.

REFERENCES

(1) de Gennes, P. G. *Scaling Concepts in Polymer Physics*: Cornell University Press: New York, 1979.

(2) Doi, M.; Edwards, S. F. *The Theory of Polymer Dynamics*: Oxford University Press: Oxford, U.K., 1986.

(3) Wool, R. P. *Polymer Interfaces: Structure and Strength*: Hanser Gardner Publications: New York, 1995.

(4) Mansfield, T.; Composto, R. J.; Stein, R. S. In *Characterization of Polymers*; Tong, H.-M., Kowalczyk, S. P., Saraf, R., Chou, N. J., Eds.; Momentum Press: New York, 2010; p 244.
(5) Composto, R. J.; Walters, R. M.; Genzer, J. *Mater. Sci. Eng. R* **2002**, *38*, 107–180.
(6) Chaturvedi, U. K.; Steiner, U.; Zak, O.; Krausch, G.; Klein, J. *Phys. Rev. Lett.* **1989**, *63*, 616–619.
(7) Reiter, G.; Steiner, U. *J. Phys II* **1991**, *1*, 659–671.
(8) Whitlow, S. J.; Wool, R. P. *Macromolecules* **1989**, *22*, 2648–2652.
(9) Whitlow, S. J.; Wool, R. P. *Macromolecules* **1991**, *24*, 5926–5938.
(10) Zhao, X.; Zhao, W.; Sokolov, J.; Rafailovich, M. H.; Schwarz, S. A.; Wilkens, B. J.; Jones, R. A. L.; Kramer, E. J. *Macromolecules* **1991**, *24*, 5991–5996.
(11) Yokoyama, H.; Kramer, E. J.; Hajduk, D. A.; Bates, F. S. *Macromolecules* **1999**, *32*, 3353–3359.
(12) Kawaguchi, D.; Tanaka, K.; Takahara, A.; Kajiyama, T. *Macromolecules* **2001**, *34*, 6164–6166.
(13) Kawaguchi, D.; Tanaka, K.; Kajiyama, T.; Takahara, A.; Tasaki, S. *Macromolecules* **2003**, *36*, 1235–1240.
(14) Lin, H. C.; Tsai, I. F.; Yang, A. C.-M.; Hsu, M. S.; Ling, Y. C. *Macromolecules* **2003**, *36*, 2464–2474.
(15) Hartson, S. E.; Stevie, F. A.; Spontak, R. J.; Koga, T.; Rafailovich, M. H.; Sokov, J. C.; Ade, H. *Polymer* **2005**, *46*, 10173–10179.
(16) Kawaguchi, D.; Masuoka, K.; Takano, A.; Tanaka, K.; Nagamura, T.; Torikai, N.; Dalgliesh, R. M.; Langridge, S.; Matsushita, Y. *Macromolecules* **2006**, *39*, 5180–5182.
(17) Harton, S. E.; Zhu, Z. M.; Stevie, F. A.; Aoyama, Y.; Ade, H. *Anal. Chem.* **2007**, *79*, 5358–5363.
(18) Karim, A.; Mansour, A.; Felcher, G. P.; Russell, T. P. *Phys. Rev. B* **1990**, *42*, 6846–6849.
(19) Russell, T. P.; Deline, V. R.; Dozier, W. D.; Felcher, G. P.; Agrawal, G.; Wool, R. P.; Mays, J. W. *Nature* **1993**, *365*, 235–237.
(20) Karim, A.; Felcher, G. P.; Russell, T. P. *Macromolecules* **1994**, *27*, 6973–6979.
(21) Agrawal, G.; Wool, R. P.; Dozier, W. D.; Felcher, G. P.; Zhou, J.; Pispas, S.; Mays, J. W.; Russell, T. P. *J. Polym. Sci., Part B* **1996**, *34*, 2919–2940.
(22) Wu, W. L.; Wallace, W. E.; van Zanten, J. H.; Bauer, B. J.; Liu, D. W.; Wong., A. *Polymer* **1997**, *38*, 2583–2594.
(23) Welp, K. A.; Wool, R. P.; Satija, S. K.; Pispas, S.; Mays, J. *Macromolecules* **1998**, *31*, 4915–4925.
(24) Lin, E. K.; Kolb, R.; Satija, S. K.; Wu, W.-L. *Macromolecules* **1999**, *32*, 3753–3757.
(25) Welp, K. A.; Wool, R. P.; Agrawal, G.; Satija, S. K.; Pispas, S.; Mays, J. *Macromolecules* **1999**, *32*, 5127–5138.
(26) Bucknall, D. G.; Butler, S. A.; Higgins, J. S. *Macromolecules* **1999**, *32*, 5453–5456.
(27) Bucknall, D. G.; Higgins, J. S.; Butler, S. A. *Chem. Eng. Sci.* **2001**, *56*, 5473–5483.
(28) Koga, T.; Seo, Y. S.; Hu, X.; Shin, K.; Zhang, Y.; Rafailovich, M. H.; Sokolov, J. C.; Chu, B.; Satija, S. K. *Europhys. Lett.* **2002**, *60*, 559–565.
(29) Gupta, R. R.; Lavery, K. A.; Francis, T. J.; Webster, J. R. P.; Smith, G. S.; Russell, T. P.; Watkins, J. J. *Macromolecules* **2003**, *36*, 346–352.
(30) Harada, M.; Suzuki, T.; Ohya, M.; Kawaguchi, D.; Takano, A.; Matsushita, Y.; Torikai, N. *J. Polym. Sci., Part B: Polym. Phys.* **2005**, *43*, 1486–1494.
(31) Klein, J.; Briscoe, B. J. *Proc. R. Soc. (London) A* **1979**, *365*, 53–73.
(32) Jordan, E. A.; Ball, R. C.; Donald, A. M.; Fetters, L. J.; Jones, R. A. L.; Klein, J. *Macromolecules* **1988**, *21*, 235–239.
(33) Composto, R.; Kramer, E. J. *J. Mater. Sci.* **1991**, *26*, 2815–2822.
(34) Jablonski, E. L.; Gorga, R. E.; Narasimhan, B. *Polymer* **2003**, *44*, 729–741.
(35) Composto, R. J.; Mayer, J. W.; Kramer, E. J.; White, D. M. *Phys. Rev. Lett.* **1986**, *57*, 1312–1315.
(36) Composto, R. J.; Kramer, E. J.; White, D. M. *Nature* **1987**, *328*, 234–236.
(37) Nelson, A. *J. Appl. Crystallogr.* **2006**, *39*, 273–276.
(38) Smith, G. S.; Majewski, J. *Proceedings of the 15th Meeting of the International Collaboration on Advanced Neutron Sources*, November 6−9, 2000, Tsukuba: Japan, 2001; Vol. 1, p 437.
(39) Mitamura, K.; Yamada, N. L.; Sagehashi, H.; Seto, H.; Torikai, N.; Sugita, T.; Furusaka, M.; Takahara, A. *J. Phys.: Conf. Ser.* **2011**, *272*, 012017.
(40) Jabbari, E.; Peppas, N. A. *Polymer* **1995**, *36*, 575–586.
(41) Londono, J. D.; Narten, A. H.; Wignall, G. D.; Honnell, K. G.; Hsieh, E. T.; Johnson, T. W.; Bates, F. S. *Macromolecules* **1994**, *27*, 2864–2871.
(42) Mark, J. E., Ed. *Physical Properties of Polymers Handbook*; Springer Science: New York, 2007, Chapter 7; p 94.
(43) Pochan, D. J.; Lin, E. K.; Satija, S. K.; Wu, W. L. *Macromolecules* **2001**, *34*, 3041–3045.
(44) Bates, F. S.; Wignall, G. D. *Phys. Rev. Lett.* **1986**, *57*, 1429–1432.
(45) de Gennes, P. G. *J. Chem. Phys.* **1980**, *72*, 4756–4763.
(46) Kramer, E. J.; Green, P. F.; Palmstrøm, C. J. *Polymer* **1984**, *25*, 473–480.
(47) Green, P. F.; Kramer, E. J. *Macromolecules* **1986**, *19*, 1108–1114.
(48) Crank, J.; *The Mathematics of Diffusion*, 2nd ed.; Oxford University Press: Oxford U.K., 1975.
(49) Sauer, B. B.; Walsh, D. J. *Macromolecules* **1991**, *24*, 5948–5955.
(50) Qiu, H.; Bousmina, M. *Macromolecules* **2000**, *33*, 6588–6594.
(51) Zhao, R.; Macosko, C. W. *AIChE J.* **2007**, *53*, 978–985.
(52) Boiko, Y. M.; Prud'homme, R. E. *Macromolecules* **1998**, *31*, 6620–6626.
(53) Boiko, Y. M.; Lyngaae-Jørgensen, J. *Polymer* **2004**, *45*, 8541–8549.
(54) Akabori, K.; Baba, D.; Koguchi, K.; Tanaka, K.; Nagamura, T. *J. Polym. Sci., B: Polym. Phys.* **2006**, *44*, 3598–3604.